Water-Soluble Iron(IV)-Oxo Complexes Supported by Pentapyridine Ligands: Axial Ligand Effects on Hydrogen Atom and Oxygen Atom Transfer Reactivity

Teera Chantarojsiri,[†] Yujie Sun,[†,∥,#] Jeffrey R. Long,*[,†,⊥] and Christopher J. Chang*[,†,‡,§,∥]

[†]Departments of Chemistry and [‡]Molecular and Cell Biology and the [§]Howard Hughes Medical Institute, University of California, Berkeley, California 94720, United States

[∥]Chemical Sciences and [⊥]Materials Sciences Divisions, Lawrence Berkeley National Laboratory, Berkeley, California 94720, United States

[#]Department of Chemistry and Biochemistry, Utah State University, Logan, Utah 84322, United States

S *Supporting Information*

ABSTRACT: We report the photochemical generation and study of a family of water-soluble iron(IV)-oxo complexes supported by pentapyridine PY5Me₂-X ligands (PY5Me₂ = 2,6-bis(1,1-bis(2-pyridyl)ethyl)pyridine; X = CF₃, H, Me, or NMe₂), in which the oxidative reactivity of these ferryl species correlates with the electronic properties of the axial pyridine ligand. Synthesis of a systematic series of $[Fe^{II}(L)(PY5Me_2\text{-}X)]^{2+}$ complexes, where L = CH₃CN or H₂O, and characterizations by several methods, including X-ray crystallography, cyclic voltammetry, and Mössbauer spectroscopy, show that

increasing the electron-donating ability of the axial pyridine ligand tracks with less positive Fe(III)/Fe(II) reduction potentials and quadrupole splitting parameters. The Fe^{II} precursors are readily oxidized to their Fe(IV)-oxo counterparts using either chemical outer-sphere oxidants such as CAN (ceric ammonium nitrate) or flash-quench photochemical oxidation with $[Ru(bpy)_3]^{2+}$ as a photosensitizer and K₂S₂O₈ as a quencher. The Fe(IV)-oxo complexes are capable of oxidizing the C−H bonds of alkane (4-ethylbenzenesulfonate) and alcohol (benzyl alcohol) substrates via hydrogen atom transfer (HAT) and an olefin (4-styrenesulfonate) substrate by oxygen atom transfer (OAT). The $[Fe^{IV}(O)(PY5Me_2\text{-}X)]^{2+}$ derivatives with electron-poor axial ligands show faster rates of HAT and OAT compared to their counterparts supported by electron-rich axial donors, but the magnitudes of these differences are relatively modest.
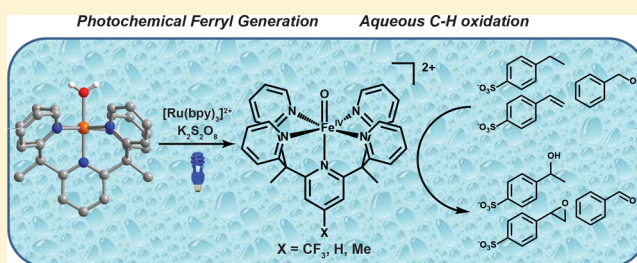
■ INTRODUCTION

High-valent iron-oxo intermediates play important roles in chemical and biological oxidations.[1−15] Iron coordinated within heme- and non-heme-dependent enzyme active sites are capable of a diverse array of oxidative transformations, including hydrogen atom transfer (HAT) from and oxygen atom transfer (OAT) to hydrocarbon substrates, as well as oxidation of phosphines, sulfides, and amines.[15−22] This rich reactivity continues to inspire the development of synthetic analogues, particularly Fe(IV)-oxo moieties with $S = 1$[23−36] or $S = 2$ spin states.[37−43] In contrast to their enzymatic counterparts, however, a vast majority of biomimetic Fe(IV)-oxo complexes have been prepared and studied in organic solution. Inspired by the wealth of elegant synthetic chemistry using amine- and pyridine-based ligands for supporting ferryl intermediates, for example, cyclam,[23,24,31,36,44] N4PY,[26] BnTPEN,[45] Me₂TACN-Py₂,[46] BP1, and BP2,[28,47,48] as well as our laboratories' work on the development of water-soluble molecular catalysts for reduction of protons to hydrogen,[49−52] we sought to expand the palette of this synthetic chemistry to aqueous media.

In this report, we present the chemical and photochemical generation, spectroscopy, and reactivity of water-soluble Fe(IV)-oxo complexes supported by an isostructural family of pentapyridine ligands where the electronic properties of the axial pyridine *trans* to the oxo moiety can be tuned in a systematic fashion. This series of compounds allows us to probe axial ligand effects on ferryl reactivity in water, which is of fundamental interest with regard to both heme and non-heme systems.[4,27,31,32,53−58] Indeed, in one notable study from the bioinorganic model literature, evaluation of [FeTMC-(MeCN)₂]²⁺ (TMC = tetramethylcyclam) complexes with a variety of anionic axial ligands (OH⁻, CF₃CO⁻, N₃⁻, NCS⁻, NCO⁻) in organic solution show that the rates of OAT reactions decrease with increasing electronic density, whereas HAT reactivity increases with more electron-rich ligands.[4,27,30,31] Here, we provide a complementary set of data on axial ligand effects of neutral pyridine donors on ferryl

reactivity in aqueous solution, focusing on OAT and HAT reactivity with hydrocarbon substrates.

■ RESULTS AND DISCUSSION

Fe(II)-PY5Me$_2$ Complexes with Varying Electronic Properties. We reasoned that varying substituents on the *para* position of the axial pyridine in a PY5Me$_2$ scaffold would directly tune electron density in the d$_{z^2}$ orbital and hence allow us to evaluate the influence of these electronic changes on Fe−oxo bonding and reactivity. As a first step toward this goal, we synthesized a series of Fe(II)-PY5Me$_2$-X complexes (where X = CF$_3$, H, Me, or NMe$_2$) with a span of electron-donating and electron-withdrawing groups (Scheme 1). Mixing equimolar

Scheme 1. Synthesis of [Fe^{II}(L)(PY5Me$_2$-X)]$^{2+}$, 1-X, and 2-X^a
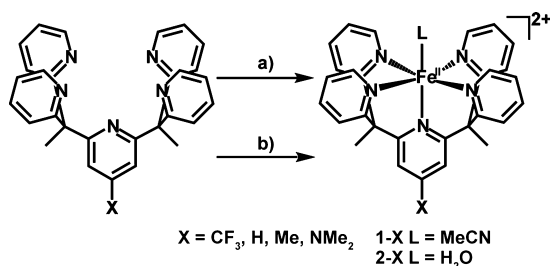
^{a}(a) Fe(OTf)$_2$ in MeCN yielded [Fe^{II}(MeCN)(PY5Me$_2$-X)](OTf)$_2$. (b) Fe(OH$_2$)$_6$(BF$_4$)$_2$ in acetone/water mixture yielded [Fe^{II}(OH$_2$)-(PY5Me$_2$-X)](BF$_4$)$_2$.

amounts of Fe(OTf)$_2$ and ligand in MeCN at room temperature yields the compounds [Fe^{II}(MeCN)(PY5Me$_2$-X)](OTf)$_2$ (**1-X**, X = CF$_3$, H, Me, NMe$_2$). As expected, the complexes are low-spin d^6 and diamagnetic ($S = 0$) and can be readily characterized by NMR spectroscopy. Crystal structures show that the **1-X** series of complexes show high structural similarity, as evidenced by their Fe−N bond lengths and N−Fe−N bond angles (Figure 1). Upon dissolution of the compounds **1-X** in water or when [Fe^{II}(OH$_2$)$_6$](BF$_4$)$_2$ was used as a starting material, the corresponding [Fe^{II}(OH$_2$)-(PY5Me$_2$)]$^{2+}$ complexes (**2-X**, X = CF$_3$, H, Me, NMe$_2$) were obtained (Scheme 1). Similar to what is observed for their

Fe(II)-acetonitrile counterparts, crystal structures of the Fe(II)-aqua complexes show comparable Fe−N bond lengths within the series (Figure 1). During the preparation of this manuscript, **2-NMe$_2$** was reported as a potential MRI contrast agent.[59]

Despite structural similarities between the different derivatives, cyclic voltammetry measurements on complexes **1-X** reveal that the Fe(III/II) redox potentials in MeCN solution can vary by up to 300 mV between the most electron-withdrawing (**1-CF$_3$**, +0.86 V vs SCE) and electron-donating (**1-NMe$_2$**, +0.56 V vs SCE) congeners. Overall, the Fe(III/II) redox potentials correlate well with the Hammett parameter (σ_p)[60] of the added substituents (Figure 2 and Table 1), where electron-rich derivatives are more easily oxidized from Fe(II) to Fe(III).
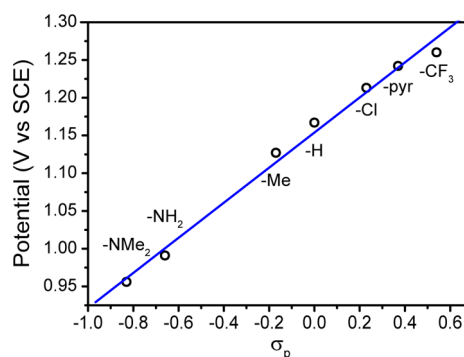
Figure 2. Linear free energy relationship of Fe(III/II) redox couples of **1-X** and Hammett Parameters (σ_p) with ρ 2.24 × 10^{-1}, $R^2 = 0.99$. Fe(III/II) redox couples were measured with 1 mM of **1-X** in 0.1 M NBu$_4$PF$_6$ in MeCN using glassy carbon as a working electrode, Ag/AgCl as a reference electrode, and Pt wire as a counter electrode. Ferrocene was used as an external standard, and the potential was corrected to vs SCE by addition of 0.4 V. Experimental details on the synthesis of **1-pyr**, **1-Cl**, and **1-NH$_2$** can be found in the Supporting Information. Pyr = 2,5-dimethylpyrrole.

The Fe(II)-aqua series, **2-X**, exhibit a similar trend, with the Fe(III/II) redox potential of the NMe$_2$ derivative being 200 mV more negative than that of the CF$_3$ derivative (Figure 3, top). Moreover, the Fe$^{III/II}$ redox potentials of these aqua complexes show a linear dependence on pH with a slope of 59 mV/pH within the pH 3−6 range, establishing that the redox process is proton-coupled and likely involves conversion of the Fe(II)-OH$_2$ to an Fe(III)-OH species, akin to what Stack and co-workers observed in related FePY$_5$ models for lipoxygenases.[61,62] In the case of the NMe$_2$ derivative, the Fe(III/II) potential is negative enough to allow oxidation of **2-NMe$_2$** by molecular oxygen, consistent with a previous study reporting that **2-NMe$_2$** has a spin-crossover transition at room temperature, which enables its reactivity with oxygen.[59]

We also evaluated the effects of varying the electronics of the axial pyridine ligand in the **1-X** and **2-X** series using Mössbauer spectroscopy. Although the isomer shifts of all Fe(II) complexes are similar, the quadrupole splitting values ($|\Delta E_q|$) rise with increasing the electron-donating ability of the ligand platform, establishing the influence of the ancillary ligand on the nuclear quadrupole moments at the iron centers (Table 2).[63]

Chemical Oxidation of Fe(II)-Aquo PY5Me$_2$ Complexes to Fe(IV)-Oxo Species. Initial attempts to generate [Fe^{IV}(O)(PY5Me$_2$)]$^{2+}$ species centered on the oxidation of **1-X** complexes in MeCN by traditional OAT reagents such as PhIO
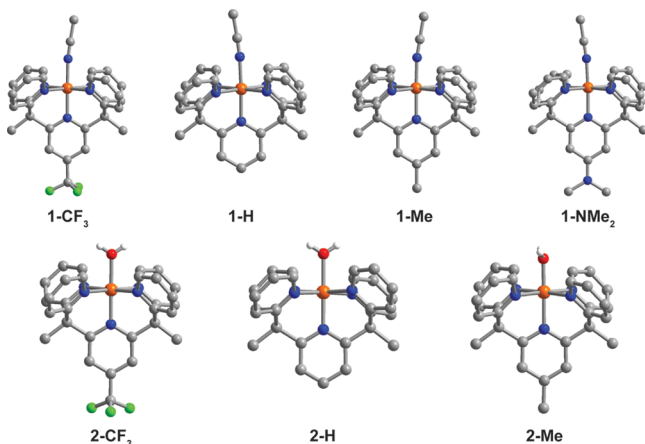

Figure 1. Crystal structures of **1-X** and **2-X**. Anions and hydrogen atoms are omitted for clarity, except for OH groups. Orange, blue, red, gray, green, and white represent Fe, N, O, C, F, and H, respectively. Structure of **2-NMe$_2$** was reported previously.[59]

Table 1. Fe(III)/Fe(II) Reduction Potentials of 1-X and 2-X in MeCN and Water, Respectively

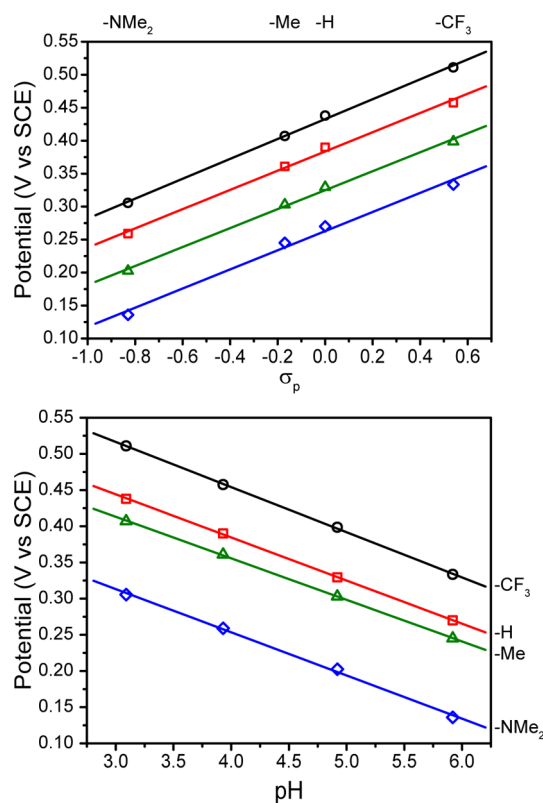|		Fe(III/II) potential (V vs SCE) of **2-X** at different pH values in water			
X	Fe(III/II) potential (V vs SCE) of **1-X** in MeCN	3	4	5	6
CF_3	1.260	0.511	0.458	0.399	0.334
H	1.167	0.438	0.390	0.330	0.270
Me	1.127	0.407	0.361	0.303	0.245
NMe_2	0.956	0.306	0.259	0.203	0.136

Figure 3. Linear free energy relationship of Fe(III/II) redox couples of **2-X** in water with ρ of 1.51×10^{-1}, $R^2 = 0.99$ (pH 3); 1.46×10^{-1}, $R^2 = 0.99$ (pH 4); 1.48×10^{-1}, $R^2 = 0.99$ (pH 5); 1.45×10^{-1}, $R^2 = 0.99$ (pH 6). The Fe(III/II) redox couples were measured with 1 mM of **2-X** in 0.1 M potassium acetate (KOAc) buffer at pH 3−6, using glassy carbon as a working electrode, Ag/AgCl as a reference electrode, and Pt wire as a counter electrode. Black circles, red squares, green triangles, and blue diamonds represent redox potential measured at pH 3, 4, 5, and 6, respectively (top). Pourbaix diagram of **2-X** at pH 3−6 (bottom). The slopes of all lines match the theoretical value of 59 mV/pH, $R^2 = 0.99$. Black circles, red squares, green triangles, and blue diamonds represent redox potential of **2-CF₃**, **2-H**, **2-Me**, and **2-NMe₂**, respectively.

and mCPBA, based on the reported formation of an Fe(IV)-oxo species at low temperature with the related ligand PY5 (Table 3).[6,26,61] However, use of these agents, as well as other oxidants, such as persulfate or Oxone, did not yield Fe(IV)-oxo species for any of the PY5Me₂ derivatives. Likewise, hydrogen peroxide and O_2 did not react appreciably with these complexes in MeCN solution, as the Fe(III/II) redox couples of the **1-X** derivatives are significantly more positive than those of other related amine-supported Fe complexes that can be oxidized readily by PhIO (Table 3).

As such, we turned our attention to the Fe(II)-OH₂ congeners, **2-X**, as their Fe(III/II) redox couples are ∼700 mV less positive relative to the MeCN-ligated **1-X** species.

Table 2. Mössbauer Parameters of Fe(II)-PY5Me₂ Complexes of the 1-X and 2-X Series at 295 and 5 K. The Quadrupole Splitting ($|\Delta E_q|$) Values Increase with the Electron-Donating Ability

		1-X		2-X	
T (K)	X	δ	$|\Delta E_q|$	δ	$|\Delta E_q|$
295	CF_3	0.4208	0.298	0.4650	0.316
	H	0.4344	0.339	0.5003	0.344
	Me	0.4339	0.367	0.4582	0.399
	NMe_2	0.4286	0.480	0.4692	0.472
5	CF_3	0.4987	0.311	0.5346	0.307
	H	0.5189	0.336	0.5717	0.335
	Me	0.5062	0.382	0.5208	0.394
	NMe_2	0.5092	0.482	0.5723	0.468

Table 3. Comparison of Fe(III/II) Reduction Potentials of Various Fe Complexes Supported by Pyridine-Amine Ligands[a]
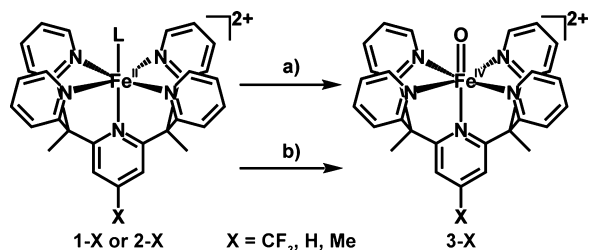
	Fe(III/II) redox couple (V vs Fc⁺/⁰)	reference
Fe^II(MeCN)(^Me₂TACN-Py₂)	0.55	6
Fe^II(MeCN)(N4PY)	0.61	26
Fe^II(MeCN)(PY5)	0.40	61
1-H	0.767	this work

[a]All but **1-H**, which exhibits the most positive potential, can be oxidized to Fe(IV)-oxo species using OAT reagents.

Cyclic voltammograms at a high scan rate of **2-X** also revealed a second redox couple, which could be attributed to the Fe(IV)/(III) redox couple (Figures S3−S6, Supporting Information). Specifically, we were encouraged by examples of Fe(IV)-oxo formation by oxidation of Fe(II)-OH₂ complexes in a proton-coupled electron transfer process, which has been achieved by chemical,[20,64] electrochemical,[29] and photochemical[46,65] means. Notably, only a few of the reported ferryl species produced in this manner have been shown to be competent for substrate oxidations in water using water itself as an OAT source, and most of these examples still require acetonitrile as an organic cosolvent.[46,65]

We were pleased to observe that the Fe(II)-OH₂ complexes **2-X** can be oxidized rapidly with CAN (ceric ammonium nitrate) in water or water/MeCN mixture, producing the corresponding pale-green Fe(IV)-oxo species (**3-X**). Oxidation of **1-X** in aqueous media also yielded the same results as the apical ligand is labile. These complexes could be observed and characterized at room temperature (Scheme 2), with the exception of the **3-NMe₂** derivative, which was only fleetingly observed at low temperature and quickly decomposed (Figure S16, Supporting Information). We speculate that autoxidation and decomposition of the ligand contributes to the instability of this intermediate. Nevertheless, the Fe(IV)-oxo species **3-CF₃**, **3-H**, and **3-Me** exhibit good stability in water in the absence of

Scheme 2. Oxidation of Fe(II)-PY5Me$_2$ Complexes to Their Fe(IV)-Oxo Counterparts by Chemical or Photochemical Routes[a]

[a](a) CAN in H$_2$O, (b) Ru(bpy)$_3$$^{2+}$, K$_2S_2O_8$, and $h\nu$ (blue light). L = H$_2$O or CH$_3$CN.

competent substrates, with half-lives of ~2 h in aqueous solution at room temperature, as determined by the decay of the characteristic weak d−d band for Fe(IV)-oxo intermediates in the UV−vis spectrum centered at ~710 nm. Interestingly, the related [Fe^{IV}(O)(PY5)]$^{2+}$ species, which contains methoxy instead of methyl groups at the methine positions supporting the pentapyridine scaffold, exhibits a reported half-life of 90 min at −65 °C in MeCN solution.[61,62]

The Fe(IV)-oxo-containing compounds, **3-CF$_3$**, **3-H**, and **3-Me**, could also be isolated in solid form when CAN oxidations were performed in 3:1 MeCN:H$_2$O solvent mixtures at higher concentrations. The isolable green-colored solid samples were characterized by Mössbauer spectroscopy, and the presence of a single Fe species confirmed complete oxidation of the Fe center (Figure 4). The observations of isomer shift values near zero mm/s are consistent with assignment to an Fe(IV) species with
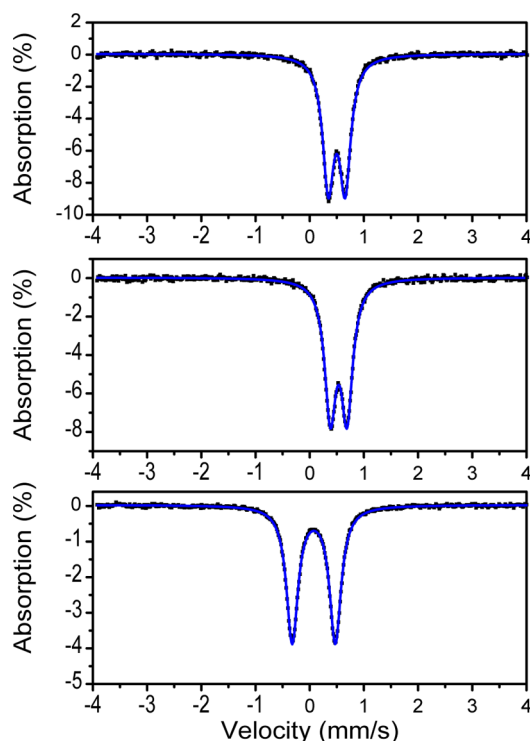
O- and N-donors in an octahedral ligand field. Moreover, the measured quadrupole splitting values at approximately 0.8 mm/s suggest a low-spin Fe(IV) ($S = 1$) configuration for all complexes. Unlike the corresponding Fe^{II}-PY5Me$_2$ species, we observe only small differences in the quadrupole splitting parameters across the [Fe^{IV}(O)(PY5Me$_2$-X)]$^{2+}$ series. Interestingly, this situation is in contrast to the axial ligand substitution studies performed on related [Fe^{IV}(O)(TMC)(X)]$^{2+}$ complexes with a wider range of anionic and neutral donors (X = MeCN, CF$_3$CO$_2$$^-$, and N$_3$$^-$), which result in relatively large differences in quadrupole splitting parameters. We rationalize the smaller magnitudes of alterations in the fitted quadrupole splitting parameters in complexes **3-X** compared to the TMC system by the more subtle fine-tuning of pyridine donor strengths on the Fe(IV)-oxo unit.[27,30,31] A summary of spectroscopic characterization parameters for Fe(IV)-oxo complexes **3-X** are listed in Table 4.

To help establish that the source of the oxo ligand is derived from water, H$_2$^{18}O was used in the oxidation reaction to synthesize the [Fe^{IV}(O)(PY5Me$_2$-X)]$^{2+}$ species. Infrared spectra of solid Fe(IV)-oxo samples generated using ^{18}O-labeled water show expected peak shifts in the Fe−O vibrations, in agreement with a harmonic oscillator model (Table 3, Figure 5). Across this homologous series, the Fe−O bond for the **3-CF$_3$** derivative is the strongest among the three derivatives. In addition, the ^{18}O-labeled [Fe^{IV}(O)(PY5Me$_2$-X)]$^{2+}$ species generated was subjected to mass spectrometric analysis. As the oxygen in the ferryl moiety is susceptible to facile exchange with oxygen from trace H$_2$^{16}O in the solvent, H$_2$^{18}O was employed as a solvent during the oxidation reaction and subsequent spectrosopic characterization. High-resolution ESI-MS data show the expected shift in m/z of 1 Da for the [Fe^{IV}(O)(PY5Me$_2$-X)]$^{2+}$ dication fragment (Figure 6).

Photochemical Oxidation of Fe(II)-Aqua PY5Me$_2$ Complexes to Fe(IV)-Oxo Species. The Fe(II)-aqua complexes in **2-X** can also be oxidized to the corresponding Fe(IV)-oxo complexes (as present in **3-X**) by photochemical means. These experiments were performed using a simple 13 W blue fluorescence light bulb as an energy source and water as the solvent and oxygen-atom source, with [Ru(bpy)$_3$]$^{2+}$ as a photosensitizer and K$_2$S$_2$O$_8$ as a terminal electron acceptor. As shown in Figure 7, the same UV−vis spectrum, indicative of Fe(IV)-oxo formation, with the characteristic d−d band centered at ~710 nm, is produced under photochemical conditions, as is observed for chemical oxidation by CAN. Complete conversion to the ferryl species proceeded within 25 min of irradiation. Reaction mixtures after photolysis were subjected to mass spectrometry, and [Fe^{IV}(O)(PY5Me$_2$-X)]$^{2+}$ intermediates, where X = CF$_3$, H, and Me, were detected directly (Table S3, Supporting Information). Moreover, in control experiments performed in the absence of light, photosensitizer, and/or terminal electron acceptor, no evidence for Fe(IV)-oxo formation was apparent.

We speculate that initial oxidation of the Fe(II)-OH$_2$ starting material to Fe(III)-OH and subsequent oxidation to Fe(IV)-oxo is a logical pathway, as Fe(IV)-oxo, directly generated in the presence of Fe(II) starting material, can undergo an intermolecular reaction to produce a μ-oxo Fe^{III} sink that cannot be oxidized to Fe(IV)-oxo. A similar pathway for the generation of Fe^{IV}(O)(^{Me_2}Py$_2$TACN) has been proposed.[46] We suggest that the initial oxidation of Fe(II)-OH$_2$ to Fe(III)-OH proceeds via K$_2$S$_2$O$_8$, which is in excess under these photochemical conditions, and subsequent oxidation of Fe-

Figure 4. Zero-field Mössbauer spectra of solid **1-CF$_3$** (top), **2-CF$_3$** (middle), and **3-CF$_3$** (bottom) (black squares) acquired at 5 K. A least-squares fit (blue line) provided the parameters listed in Tables 2 and 4.

Table 4. Mössbauer, UV–Visible, and Infrared Spectroscopic Parameters for Fe(IV)-Oxo PY5Me$_2$ Complexes 3-X

	δ ($|\Delta E_q|$) (mm/s) at 5 K	λ_{max} (nm) (ε, M^{-1} cm^{-1})	ν(Fe=^{16}O), ν(Fe=^{18}O) (cm^{-1})
3-CF$_3$	0.0782 (0.800)	710 (300)	841, 807
3-H	0.0820 (0.795)	712 (310)	821, 785
3-Me	0.0785 (0.718)	713 (300)	822, 786
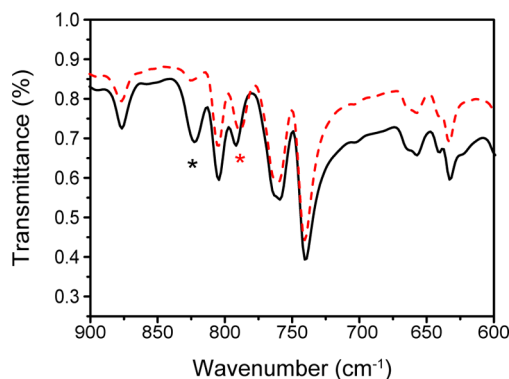
Figure 5. Infrared absorption spectra of the Fe(IV)-oxo PY5Me$_2$ complex **3-Me** synthesized from H$_2$^{16}O (black) and H$_2$^{18}O (red). Asterisks denote the Fe–oxo vibration ν(Fe-O). Difference spectra are shown in Figure S23 (Supporting Information).
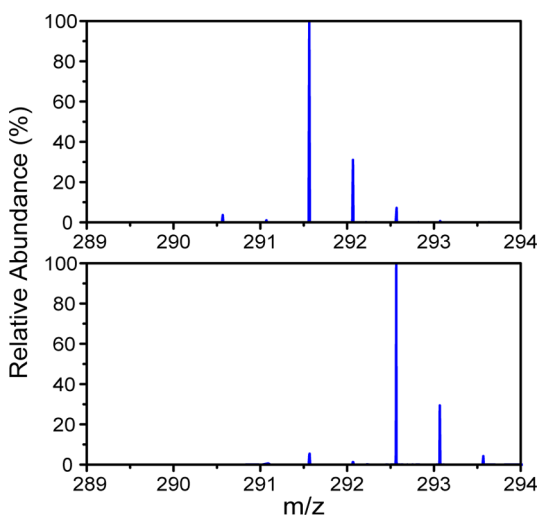

Figure 6. Mass spectra of **3-CF$_3$-^{16}O** and **3-CF$_3$-^{18}O**. A mass shift of $m/z = 1$ Da was observed when H$_2$^{18}O is employed, consistent with water as the source of the oxo ligand.
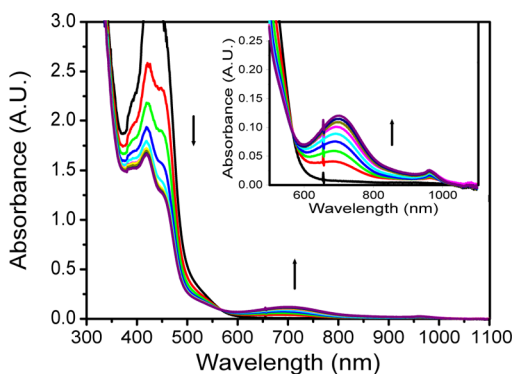

Figure 7. Photochemical oxidation of Fe(II)-aqua **2-CF$_3$** to Fe(IV)-oxo **3-CF$_3$** in water using a flash-quench [Ru(bpy)$_3$]$^{2+}$/K$_2$S$_2$O$_8$ system.

(III)-OH to Fe(IV)-oxo occurs by [Ru(bpy)$_3$]$^{2+}$-initiated photochemistry. Indeed, **2-X** can react with K$_2$S$_2$O$_8$ (Figure S13, Supporting Information), as shown by UV–vis spectroscopy, and Mössbauer spectroscopy of the resulting species reveals an isomer shift of 0.23 mm/s, consistent with an Fe^{III} species (Figure S9, Supporting Information). Given the facile proton-coupled oxidation of the complexes in **2-X**, as shown by cyclic voltammetry, we tentatively propose that K$_2$S$_2$O$_8$ oxidation of the Fe(II)-aqua complexes generates their putative Fe(III)-hydroxide counterparts.

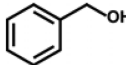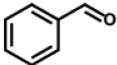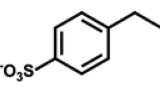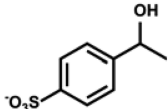**Oxidative Reactivity of Photochemically Generated Fe(IV)-Oxo PY5Me$_2$ Species: Electron-Withdrawing Axial Pyridines Increase Rates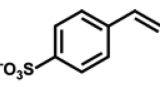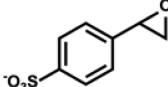 of Both HAT and OAT Reactions.** With a systematic series of [Fe^{IV}(O)(PY5Me$_2$-X)]$^{2+}$ species in hand, we surveyed their oxidative reactivity for HAT and OAT reactions with hydrocarbons and alcohols, to benchmark their properties compared to other synthetic $S = 1$ Fe(IV)-oxo complexes reported in the literature. Stoichiometric reactivity studies of the Fe(IV)-oxo complexes in **3-CF$_3$**, **3-H**, and **3-Me** in MeCN solution, isolated from chemical oxidation, show rapid reaction with hydrocarbon substrates containing weak C–H bonds, including 9,10-dihydroanthracene (BDE = 77 kcal/mol) and ethylbenzene (87 kcal/mol).[2,42] The ferryl species are also competent for oxidation of benzyl alcohol to benzaldehyde, as well as oxidation of N,N-dimethylaminobenzene; the latter result provides a rationale for the relative instability of **3-NMe$_2$**, suggesting that ligand oxidation can lead to formation of an Fe^{III} byproduct.

We also observe that the [Fe^{IV}(O)(PY5Me$_2$-X)]$^{2+}$ species are capable of hydrocarbon oxidations in aqueous solution at pH 5.5 (nonbuffered water), expanding their use beyond organic media. Specifically, we evaluated three water-soluble substrates to represent different modes of reactivity:[25] benzyl alcohol for HAT-mediated alcohol oxidation, 4-ethylbenzenesulfonate sodium salt for HAT-mediated hydrocarbon oxidation, and 4-styrenesulfonate sodium salt for olefin oxidation via OAT. Fe(IV)-oxo generated photochemically reacted with 1 equiv of substrate. After 5 min, d_4-sodium trimethylsilylpropanoate was added as an internal standard.[66] The products of the oxidation reaction were identified using NMR spectroscopy, and the results showed oxidation of benzyl alcohol to benzaldehyde, ethylbenzenesulfonate to 1-phenylethanolsulfonate and acetophenonesulfonate, and styrenesulfonate to styreneoxidesulfonate and the corresponding diol products.

Second-order rate constants were measured by observing decay of the characteristic Fe(IV)-oxo signature centered at 710 nm in the UV–vis spectra upon substrate oxidation. The Fe(IV)-oxo species were generated under photochemical conditions before addition of 5, 10, 20, 30, and 40 equiv of substrate. Among this systematic series, we observe that the [Fe^{IV}(O)(PY5Me$_2$-X)]$^{2+}$ derivative containing the most electron-withdrawing group, the **3-CF$_3$** congener, shows the fastest rates of oxidation for both HAT and OAT reactions with the substrates tested (Table 5).

Reaction rate differences also correlate to the Hammett parameters (σ_p) of the ligand substituents, as shown in Figure

Table 5. Second-Order Rate Constants of Substrate Oxidation by $Fe^{IV}(O)PY5Me_2$ Species 3-X at 25 °C in Aqueous Solution at pH 5.5 (Nonbuffered Water)

Substrate	Major Product	k_2 (mM^{-1} s^{-1}) (x 10^{-4})		
		3-CF$_3$	3-H	3-Me
benzyl alcohol	benzaldehyde	29.4 ± 3.5	12.4 ± 3.0	7.60 ± 1.57
4-ethylbenzenesulfonate		49.7 ± 9.5	17.5 ± 1.8	7.86 ± 1.29
4-styrenesulfonate	epoxide	1.58 ± 0.18	0.740 ± 0.105	0.750 ± 0.150

8, with a slope (ρ) of 0.79 (benzyl alcohol), 1.06 (ethylbenzenesulfonate), and 0.49 (styrenesulfonate). The
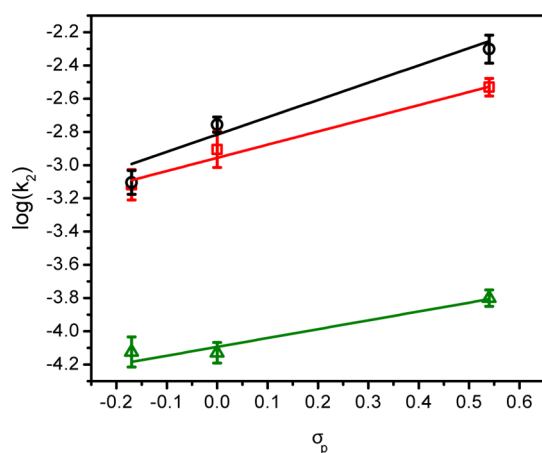

Figure 8. Linear free energy relationship of oxidation reaction rate constants (pseudo-first-order) of hydrocarbon substrates by **3-X** and Hammett parameters (σ_p). Black squares, red circles, and green triangles represent oxidation rate of benzyl alcohol (ρ 0.79, $R^2 = 0.98$), 4-ethylbenzenesulfonate (ρ 1.06, $R^2 = 0.95$), and 4-styrenesulfonate (ρ 0.49, $R^2 = 0.94$), respectively.

oxidation rate enhancement by the electron-withdrawing substituent is moderate compared to the axial ligand effect of the anionic ligand demonstrated in the non-heme model complex, $Fe^{IV}(O)(TMC)$,[30,31] and to the $Fe^{IV}(O)(TMP^{+\bullet})$[58] and $Mn^V(O)(TBP_8Cz)$[55−57] systems. While those systems reported orders-of-magnitude increase in reaction rate, the change in substituents serves as a fine-tuning to the electronic properties and varies the reaction rate by less than 10-fold. Small variations in Mössbauer parameters (Table 4) and redox potentials measured by voltammetry (Figures S3−S6, Supporting Information) also support this finding. DFT calculation study is currently employed to better understand structure−reactivity relationships.

■ CONCLUDING REMARKS

Through the synthesis, characterization, and evaluation of a family of Fe-PY5Me$_2$-X complexes, we have probed the effect of systematic changes on the axial pyridine ligand toward the electronic properties and reactivity of water-soluble Fe(IV)-oxo species supported by this pentapyridine platform. Substitutions at the *para* position of the axial pyridine with an array of electron-donating and electron-withdrawing functionalities result in a predictable and significant 200−300 mV shift in the $Fe^{III/II}$ redox potentials, with concomitant changes in the quadrupole splitting parameters observed in the Mössbauer spectra. Oxidations of Fe(II)-aqua precursors by chemical or photochemical means proceed smoothly to generate water-soluble Fe(IV)-oxo complexes with competent lifetimes at room temperature; as expected across the series, electron-rich derivatives are more readily oxidized to the Fe(IV)-oxo species. Identification and characterization of the ferryl species was probed by multiple techniques, including *in situ* UV−vis, Mössbauer, and infrared spectroscopies, as well as analysis of ^{18}O-labeled products. The data reveal a correlation between axial ligand donor strength and ferryl reactivity within a structurally homologous series, but the effect is small in magnitude. The Fe(IV)-oxo complex **3-CF$_3$**, which contains the most electron-poor axial ligand synthesized in this series, showed the weakest Fe−O bond and the fastest rate with a variety of HAT and OAT substrates. Taken together, this study provides a unique family of synthetic, water-soluble Fe(IV)-oxo complexes with systematic electronic tuning of axial ligands with high structural similarity. Current and future efforts will further exploit the versatility of PY5Me$_2$ and related polypyridine platforms for catalytic oxidation and reduction reactions in green, aqueous media.

■ EXPERIMENTAL SECTION

General Synthetic and Physical Methods. All manipulations were performed under ambient conditions, unless otherwise noted. Pyrophoric reagents were handled using standard glovebox and Schlenk-line techniques. Milli-Q H$_2$O was used in all experiments. All commercially available reagents were used without further purification, unless otherwise noted. PY5Me$_2$ (2,6-bis(1,1-bis(2-pyridyl)ethyl)-pyridine), PY5Me$_2$-CF$_3$, and PY5Me$_2$-NMe$_2$ were synthesized according to literature procedures[51] with slight modification. UV−vis spectra were recorded using a Varian Cary 50 BIO and an Agilent 8453 UV−visible spectrometer, both equipped with a Unisoku cryostat. Infrared spectra were recorded using a Bruker FT-IR Alpha-P ATR Instrument. Measurements of pH were conducted using a Thermo Orion 420 A+. NMR experiments were conducted using Bruker AVB-400 and AV-600 spectrometers. ESI-MS experiments were performed by the QB3 Proteomics/Mass Spectrometry facility at the University of California, Berkeley. X-ray crystallography was performed in the Chexray facility at the University of California, Berkeley. Elemental analyses were conducted at the Microanalytical Laboratory of the University of California, Berkeley.

PY5Me$_2$-Me. An *n*-BuLi solution (4 mL, 2.5 M, 10 mmol, 3 equiv) was added slowly to a solution of 1,1-dipyridylethane (1.86 g, 10 mmol, 3 equiv) in 40 mL of dry and degassed 1,4-dioxane at 0 °C. The solution was stirred for 30 min before 2,6-dichloro-4-picoline (0.545 g, 3.36 mmol, 1 equiv) was added as a solid. The reaction mixture was allowed to warm to room temperature and then heated to reflux for 2 days. After the solution was allowed to cool to room temperature, water was added to quench the reaction. The product was extracted with dichloromethane (3 × 20 mL). The organic layer was separated, washed with brine (2 × 15 mL), and dried with Na$_2$SO$_4$. The solvent was removed *in vacuo*. Methanol was added, followed by rotary evaporation to remove residual 1,4-dioxane. Et$_2$O was then added to precipitate a light yellow solid. The solid was washed with Et$_2$O and dried in air. A yellow solid (1.37 g, 87.3% yield) was obtained. ^{1}H NMR (600 MHz, CDCl$_3$) δ 8.51 (d, *J* = 4.7 Hz, 4H), 7.38 (td, *J* = 7.8, 1.7 Hz, 4H), 7.04 (dd, *J* = 7.4, 5.0 Hz, 4H), 6.91 (s, 2H), 6.81 (d, *J* = 8.0 Hz, 4H), 2.24 (s, 3H), 2.19 (s, 6H). ESI-MS: *m/z* calcd for

$C_{35}H_{32}N_6$ 536.27, found 537.3 (M + 1). Calcd $C_{35}H_{32}N_6$ (536.67 g/mol): C, 78.33; H, 6.01; N, 15.66. Found: C, 78.06; H, 6.20; N, 15.49.

General Procedure for Synthesis of [Fe(MeCN)(PY5Me$_2$-X)](OTf)$_2$ Complexes (1-X). PY5Me$_2$-X ligand (100 mg, 0.186 mmol) was mixed with Fe(OTf)$_2$ (60.7 mg, 0.186 mmol) in 4 mL of MeCN. The solution color turned red upon mixing. The resulting solution was concentrated, filtered, and recrystallized by diffusing Et$_2$O into MeCN solution, yielding red needles suitable for single-crystal X-ray crystallography.

[Fe(MeCN)(PY5Me$_2$-CF$_3$)](OTf)$_2$ (1-CF$_3$). Yield: 58.9%. ^{1}H NMR (600 MHz, CD$_3$CN) δ 9.60 (d, J = 6.1 Hz, 4H), 7.97 (s, 2H), 7.76−7.70 (m, 8H), 7.36 (tt, J = 5.4, 2.3 Hz, 4H), 2.60 (s, 6H). ESI-MS: m/z calcd for $C_{32}H_{27}F_3FeN_6{}^{2+}$ 304.0794, found 304.0795 for $C_{31}H_{24}F_6Fe$-$N_5O_3S^+$ 716.0859, found 716.0828 for Calcd $C_{34}H_{27}F_6FeN_6O_6S_2$ (906.58 g·mol^{-1}): C, 45.05; H, 3.00; N, 9.27. Found: C, 45.16; H, 2.78; N, 9.53.

[Fe(MeCN)(PY5Me$_2$-H)](OTf)$_2$ (1-H). Yield: 77.8%. ^{1}H NMR (600 MHz, CD$_3$CN) δ 9.60 (d, J = 5.7 Hz, 4H), 7.81 (s, 2H), 7.72 (d, J = 4.6 Hz, 8H), 7.68 (s, 1H), 7.33 (p, J = 5.1 Hz, 4H), 2.52 (s, br, 6H). ESI-MS: m/z calcd for $C_{31}H_{28}FeN_6{}^{2+}$ 270.0857, found 270.0857; for $C_{30}H_{25}F_3FeN_5O_3S^+$ 648.0974, found 648.0952. Calcd $C_{33}H_{28}F_6Fe$-$N_6O_6S_2$ (838.58 g·mol^{-1}): C, 47.27; H, 3.37; N, 10.02. Found: C, 47.12; H, 3.37; N, 9.94.

[Fe(MeCN)(PY5Me$_2$-Me)](OTf)$_2$ (1-Me). Yield: 86.7%. ^{1}H NMR (600 MHz, CD$_3$CN) δ 9.62−9.57 (d, 4H), 7.74−7.69 (m, 8H), 7.68 (s, 2H), 7.33 (dq, J = 6.5, 4.2, 3.5 Hz, 4H), 2.52 (s, 6H), 2.29 (s, 3H). ESI-MS: m/z calcd for $C_{32}H_{36}FeN_6{}^{2+}$ 277.0942, found 277.0935; for $C_{31}H_{27}F_3FeN_5O_3S^+$ 662.1132, found 662.1110. Calcd $C_{34}H_{30}F_6Fe$-$N_6O_6S_2$ (852.61 g·mol^{-1}): C, 47.90; H, 3.55; N, 9.86. Found: C, 47.97; H, 3.55; N, 9.88.

[Fe(MeCN)(PY5Me$_2$-NMe$_2$)](OTf)$_2$ (1-NMe$_2$). Yield: 98.0%. ^{1}H NMR (600 MHz, CD$_3$CN) δ 9.58 (d, J = 5.8 Hz, 4H), 7.69 (dd, J = 17.9, 7.8 Hz, 8H), 7.32 (t, J = 6.7 Hz, 4H), 6.93 (s, 2H), 2.91 (s, 6H), 2.48 (s, 6H). ESI-MS: m/z calcd for $C_{33}H_{33}FeN_7{}^{2+}$ 291.6065 found 291.6068; for $C_{32}H_{30}F_3FeN_6O_3S^+$ 691.1382, found 691.1375. Calcd $C_{35}H_{34}F_6FeN_7O_6S_2$ (881.65 g·mol^{-1}): C, 47.68; H, 3.77; N, 11.12. Found: C, 48.00; H, 3.78; N, 11.34.

General Procedure for Synthesis of [Fe(OH$_2$)(PY5Me$_2$-X)]-(BF$_4$)$_2$ Complexes (2-X). A slurry of PY5Me$_2$-X ligand (100 mg, 0.186 mmol) in 4 mL of acetone was mixed with Fe(OH$_2$)$_6$(BF$_4$)$_2$ (60.7 mg, 0.186 mmol) in 0.5 mL of water. The solution color turned red immediately upon addition of the iron salt. The resulting solution was concentrated, filtered, and recrystallized by diffusing Et$_2$O into the resulting solution, yielding X-ray diffraction-quality red needles.

[Fe(OH$_2$)(PY5Me$_2$-CF$_3$)](BF$_4$)$_2$ (2-CF$_3$). Yield: 78.4%. Calcd $C_{30}H_{34}$-$B_2F_{11}FeN_5O_5$ (831.079 g·mol^{-1}): C, 43.36; H, 4.12; N, 8.43. Found: C, 43.75; H, 4.25; N, 8.42.

[Fe(OH$_2$)(PY5Me$_2$-H)](BF$_4$)$_2$ (2-H). Yield: 89.7%. Calcd $C_{29}H_{27}B_2F_8$-FeN_5O (691.02 g·mol^{-1}): C, 50.41; H, 3.94; N, 10.13. Found: C, 50.24; H, 3.80; N, 10.22.

[Fe(OH$_2$)(PY5Me$_2$-Me)](BF$_4$)$_2$ (2-Me). Yield: 83.5%. Calcd $C_{30}H_{37}$-$B_2F_8FeN_5O_5$ (777.11 g·mol^{-1}): C, 46.37; H, 4.80; N, 9.01. Found: C, 46.86; H, 4.85; N, 9.01.

General Procedure for Chemical Formation of [Fe^{IV}(O)-(PY5Me$_2$-X)]$^{2+}$ Complexes (3-X). 1-X or 2-X complex (40 mg, 0.047 mmol) was dissolved in 0.6 mL of 3:1 MeCN:H$_2$O. (NH$_4$)$_2$Ce(NO$_3$)$_6$ (137 mg, 0.25 mmol) was added as a solid. The mixture was sonicated for 30 s and placed in an ice bath as a green precipitate formed. The solid was collected on a sintered glass frit and washed with ice cold 3:1 MeCN:H$_2$O mixed solvent. The products were stored at −20 °C or directly used as samples for Mössbauer, IR spectroscopy, and mass spectrometry. For UV−vis experiments, a 1 mM solution of 1-X or 2-X in 4 mL of H$_2$O was prepared. 5 equiv of (NH$_4$)$_2$Ce(NO$_3$)$_6$ was added as a solid into a quartz cuvette equipped with a stir bar for rapid stirring. Absorption at 710 nm was monitored as the reaction progressed to completion. For O-18 labeling experiments, H$_2{}^{18}$O was used a solvent during the formation of 3-X-^{18}O only.

Electrochemical Methods. Nonaqueous electrochemical experiments were conducted under an Ar atmosphere in 0.1 M NBu$_4$PF$_6$ in CH$_3$CN. Cyclic voltammetry experiments were carried out using a BASI Epsilon potentiostat with a C-3 cell stand. The working electrode was a glassy carbon disk (3.0 mm diameter), and the counter electrode was a platinum wire. A silver wire in a porous Vycor tip glass tube filled with 0.1 M NBu$_4$PF$_6$ in CH$_3$CN was used as a pseudo-reference electrode. The scan rate for all cyclic voltammograms was 100 mV/s unless otherwise noted. All potentials were referenced against ferrocenium/ferrocene as an external standard and converted to SCE by adding 0.40 V to the measured potentials. Aqueous electrochemical experiments were conducted in a similar setup except that a Ag/AgCl electrode (CH Instruments) was used as a reference electrode with no external standard.

Photochemical Studies. All photochemical studies were performed under ambient conditions with either a 13 W blue fluorescence light bulb (GE, ACE hardware) or a small blue LED (VWR International). General conditions are as follows: 0.5 mM [Fe^{II}(MeCN)(PY5Me$_2$-X)]$^{2+}$, 0.1 mM [Ru(bpy)$_3$]Cl$_2$, and 5 mM K$_2$S$_2$O$_8$. Kinetic studies were conducted with 0.5 mM [Fe^{II}(MeCN)-(PY5Me$_2$-X)]$^{2+}$, 0.1 mM [Ru(bpy)$_3$]Cl$_2$, and 10 mM K$_2$S$_2$O$_8$. Solutions were photolyzed for 10 min before 5, 10, 20, 30, and 40 equiv of substrate were added. Decay rates of absorbance at 710 nm were measured in at least triplicate.

NMR Studies. Stoichiometric reactions of Fe(IV)-oxo species and substrate were performed in 5% d_6-DMSO and 95% D$_2$O. Delay time was adjusted to 10 s. General conditions were as follows: 2 mM Fe complexes, 2 mM substrate, and 1 mM of 3-(trimethylsilyl)propionic-2,2,3,3-d_4 acid sodium salt (NaTSP) as an internal standard.[66]

General Methods for X-ray Crystallography. Single-crystal X-ray diffraction was conducted at the University of California, Berkeley, College of Chemistry, X-ray Crystallography Facility. Crystals were mounted on nylon loops in paratone-N hydrocarbon oil. All data collections were performed on either a Bruker Quazar or an APEX diffractometer equipped with a CCD area detector and a low-temperature apparatus. Data integration was performed using SAINT. Preliminary data analysis and absorption correction were performed using XPREP and SADABS. Structure solution and refinement was performed using the SHELX software package.

General Methods for Mössbauer Spectroscopy. Zero-field, ^{57}Fe Mössbauer spectra were recorded in a constant acceleration spectrometer (SEE Co., Edina, MN) between room temperature and 5 K in a Janis Research Co. cryostat (Willmington, MA). Collected spectra were analyzed using the WMOSS software package (SEE Co., Edina, MN). Isomer shifts are reported relative to α-iron (27 μm foil) at room temperature. Samples were prepared by mixing boron nitrile (BN) with finely ground crystalline samples of Fe complexes. A powder mixture was placed in a nylon washer wrapped in Kapton tape under an inert atmosphere prior to introducing into the spectrometer in air. Solution samples were prepared by freezing the Teflon sample holder containing 0.5 mL of sample in liquid nitrogen before introducing into the previously cooled spectrometer in air.

■ ASSOCIATED CONTENT

Ⓢ Supporting Information

Additional supplemental figures as labeled in the text, experimental information, and NMR spectra. The Supporting Information is available free of charge on the ACS Publications website at DOI: 10.1021/acs.inorgchem.5b00658.

■ AUTHOR INFORMATION

Corresponding Authors
*E-mail: jrlong@berkeley.edu (J.R.L.).
*E-mail: chrischang@berkeley.edu (C.J.C.).

Notes
The authors declare no competing financial interest.

■ ACKNOWLEDGMENTS

■ REFERENCES

(1) Costas, M.; Mehn, M. P.; Jensen, M. P.; Que, L., Jr. *Chem. Rev.* **2004**, *104*, 939−986.

(2) Que, L., Jr. *Acc. Chem. Res.* **2007**, *40*, 493−500.

(3) Nam, W. *Acc. Chem. Res.* **2007**, *40*, 522−531.

(4) Nam, W.; Lee, Y.; Fukuzumi, S. *Acc. Chem. Res.* **2014**, *47*, 1146−1154.

(5) Stone, K. L.; Borovik, A. S. *Curr. Opin. Chem. Biol.* **2009**, *13*, 114−118.

(6) Wang, D.; Ray, K.; Collins, M. J.; Farquhar, E. R.; Frisch, J. R.; Gomez, L.; Jackson, T. a.; Kerscher, M.; Waleska, A.; Comba, P.; Costas, M.; Que, L., Jr. *Chem. Sci.* **2012**, *4*, 282−291.

(7) Groves, J. T. J. *Inorg. Biochem.* **2006**, *100*, 434−447.

(8) Shaik, S.; Cohen, S.; Wang, Y.; Chen, H.; Kumar, D.; Thiel, W. *Chem. Rev.* **2010**, *110*, 949−1017.

(9) Krebs, C.; Galonić Fujimori, D.; Walsh, C. T.; Bollinger, J. M. *Acc. Chem. Res.* **2007**, *40*, 484−492.

(10) Holm, R. H.; Kennepohl, P.; Solomon, E. I. *Chem. Rev.* **1996**, *96*, 2239−2314.

(11) Feig, A. L.; Lippard, S. J. *Chem. Rev.* **1994**, *94*, 759−805.

(12) Wallar, B. J.; Lipscomb, J. D. *Chem. Rev.* **1996**, *96*, 2625−2658.

(13) McGown, A. J.; Kerber, W. D.; Fujii, H.; Goldberg, D. P. *J. Am. Chem. Soc.* **2009**, *131*, 8040−8048.

(14) Krishnamurthy, D.; Kasper, G. D.; Namuswe, F.; Kerber, W. D.; Narducci Sarjeant, A. A.; Moënne-Loccoz, P.; Goldberg, D. P. *J. Am. Chem. Soc.* **2006**, *128*, 14222−14223.

(15) Sahu, S.; Quesne, M. G.; Davies, C. G.; Dürr, M.; Ivanović-Burmazović, I.; Siegler, M. A.; Jameson, G. N. L.; de Visser, S. P.; Goldberg, D. P. *J. Am. Chem. Soc.* **2014**, *136*, 13542−13545.

(16) Vaillancourt, F. H.; Yeh, E.; Vosburg, D. A.; Garneau-Tsodikova, S.; Walsh, C. T. *Chem. Rev.* **2006**, *106*, 3364−3378.

(17) Baik, M.-H.; Newcomb, M.; Friesner, R. A.; Lippard, S. J. *Chem. Rev.* **2003**, *103*, 2385−2419.

(18) Gunay, A.; Theopold, K. H. *Chem. Rev.* **2010**, *110*, 1060−1081.

(19) Abouelatta, A. I.; Campanali, A. A.; Ekkati, A. R.; Shamoun, M.; Kalapugama, S.; Kodanko, J. J. *Inorg. Chem.* **2009**, *48*, 7729−7739.

(20) Ekkati, A. R.; Kodanko, J. J. *J. Am. Chem. Soc.* **2007**, *129*, 12390−12391.

(21) Cho, K.; Leeladee, P.; McGown, A. J.; DeBeer, S.; Goldberg, D. P. *J. Am. Chem. Soc.* **2012**, *134*, 7392−7399.

(22) Mandal, D.; Ramanan, R.; Usharani, D.; Janardanan, D.; Wang, B.; Shaik, S. *J. Am. Chem. Soc.* **2014**, *137*, 722−733.

(23) Bukowski, M. R.; Koehntop, K. D.; Stubna, A.; Bominaar, E. L.; Halfen, J. A.; Münck, E.; Nam, W.; Que, L., Jr. *Science* **2005**, *310*, 1000−1002.

(24) Rohde, J.-U.; In, J.-H.; Lim, M. H.; Brennessel, W. W.; Bukowski, M. R.; Stubna, A.; Münck, E.; Nam, W.; Que, L., Jr. *Science* **2003**, *299*, 1037−1039.

(25) Lim, M. H.; Rohde, J.-U.; Stubna, A.; Bukowski, M. R.; Costas, M.; Ho, R. Y. N.; Munck, E.; Nam, W.; Que, L., Jr. *Proc. Natl. Acad. Sci. U.S.A.* **2003**, *100*, 3665−3670.

(26) Klinker, E. J.; Kaizer, J.; Brennessel, W. W.; Woodrum, N. L.; Cramer, C. J.; Que, L., Jr. *Angew. Chem., Int. Ed.* **2005**, *44*, 3690−3694.

(27) Sastri, C. V.; Park, M. J.; Ohta, T.; Jackson, T. A.; Stubna, A.; Seo, M. S.; Lee, J.; Kim, J.; Kitagawa, T.; Münck, E.; Que, L., Jr.; Nam, W. *J. Am. Chem. Soc.* **2005**, *127*, 12494−12495.

(28) Bautz, J.; Bukowski, M. R.; Kerscher, M.; Stubna, A.; Comba, P.; Lienke, A.; Münck, E.; Que, L., Jr. *Angew. Chem., Int. Ed.* **2006**, *45*, 5681−5684.

(29) Collins, M. J.; Ray, K.; Que, L., Jr. *Inorg. Chem.* **2006**, *45*, 8009−8011.

(30) Sastri, C. V.; Lee, J. J.; Oh, K.; Lee, Y. J.; Lee, J. J.; Jackson, T. a; Ray, K.; Hirao, H.; Shin, W.; Halfen, J. A; Kim, J.; Que, L., Jr.; Shaik, S.; Nam, W. *Proc. Natl. Acad. Sci. U.S.A.* **2007**, *104*, 19181−19186.

(31) Jackson, T. A.; Rohde, J. U.; Mi, S. S.; Sastri, C. V.; DeHont, R.; Stubna, A.; Ohta, T.; Kitagawa, T.; Münck, E.; Nam, W.; Que, L., Jr. *J. Am. Chem. Soc.* **2008**, *130*, 12394−12407.

(32) Chanda, A.; Shan, X.; Chakrabarti, M.; Ellis, W. C.; Popescu, D. L.; Tiago de Oliveira, F.; Wang, D.; Que, L., Jr.; Collins, T. J.; Münck, E.; Bominaar, E. L. *Inorg. Chem.* **2008**, *47*, 3669−3678.

(33) Mukherjee, A.; Martinho, M.; Bominaar, E. L.; Münck, E.; Que, L., Jr. *Angew. Chem., Int. Ed.* **2009**, *48*, 1780−1783.

(34) Kim, S. O.; Sastri, C. V.; Seo, M. S.; Kim, J.; Nam, W. *J. Am. Chem. Soc.* **2005**, *127*, 4178−4179.

(35) Ray, K.; Pfaff, F. F.; Wang, B.; Nam, W. *J. Am. Chem. Soc.* **2014**, *136*, 13942−13958.

(36) Wilson, S. A.; Chen, J.; Hong, S.; Lee, Y.-M.; Clémancey, M.; Garcia-Serres, R.; Nomura, T.; Ogura, T.; Latour, J.-M.; Hedman, B.; Hodgson, K. O.; Nam, W.; Solomon, E. I. *J. Am. Chem. Soc.* **2012**, *134*, 11791−11806.

(37) Pestovsky, O.; Stoian, S.; Bominaar, E. L.; Shan, X.; Münck, E.; Que, L., Jr.; Bakac, A. *Angew. Chem., Int. Ed.* **2005**, *44*, 6871−6874.

(38) England, J.; Guo, Y.; Farquhar, E. R.; Young, V. G.; Münck, E.; Que, L., Jr. *J. Am. Chem. Soc.* **2010**, *132*, 8635−8644.

(39) Lacy, D. C.; Gupta, R.; Stone, K. L.; Greaves, J.; Ziller, J. W.; Hendrich, M. P.; Borovik, A. S. *J. Am. Chem. Soc.* **2010**, *132*, 12188−12190.

(40) MacBeth, C. E.; Golombek, A. P.; Young, V. G., Jr.; Yang, C.; Kuczera, K.; Hendrich, M. P.; Borovik, A. S. *Science* **2000**, *289*, 938−941.

(41) England, J.; Guo, Y.; Van Heuvelen, K. M.; Cranswick, M. A.; Rohde, G. T.; Bominaar, E. L.; Münck, E.; Que, L., Jr. *J. Am. Chem. Soc.* **2011**, *133*, 11880−11883.

(42) Seo, M. S.; Kim, N. H.; Cho, K.-B.; So, J. E.; Park, S. K.; Clémancey, M.; Garcia-Serres, R.; Latour, J.-M.; Shaik, S.; Nam, W. *Chem. Sci.* **2011**, *2*, 1039−1045.

(43) Bigi, J. P.; Harman, W. H.; Lassalle-Kaiser, B.; Robles, D. M.; Stich, T. A.; Yano, J.; Britt, R. D.; Chang, C. J. *J. Am. Chem. Soc.* **2012**, *134*, 1536−1542.

(44) Grapperhaus, C. A.; Mienert, B.; Bill, E.; Weyhermuller, T.; Wieghardt, K. *Inorg. Chem.* **2000**, *39*, 5306−5317.

(45) Company, A.; Prat, I.; Frisch, J. R.; Mas-Ballesté, R.; Güell, M.; Juhász, G.; Ribas, X.; Münck, E.; Luis, J. M.; Que, L., Jr.; Costas, M. *Chem.—Eur. J.* **2011**, *17*, 1622−1634.

(46) Company, A.; Sabenya, G.; González-Béjar, M.; Gómez, L.; Clémancey, M.; Blondin, G.; Jasniewski, A. J.; Puri, M.; Browne, W. R.; Latour, J.-M.; Que, L., Jr.; Costas, M.; Pérez-Prieto, J.; Lloret-Fillol, J. *J. Am. Chem. Soc.* **2014**, *136*, 4624−4633.

(47) Bukowski, M. R.; Comba, P.; Lienke, A.; Limberg, C.; Lopez de Laorden, C.; Mas-Ballesté, R.; Merz, M.; Que, L., Jr. *Angew. Chem., Int. Ed.* **2006**, *45*, 3446−3449.

(48) Comba, P.; Fukuzumi, S.; Kotani, H.; Wunderlich, S. *Angew. Chem., Int. Ed.* **2010**, *49*, 2622−2625.

(49) Bigi, J. P.; Hanna, T. E.; Harman, W. H.; Chang, A.; Chang, C. J. *Chem. Commun.* **2010**, *46*, 958−960.

(50) Karunadasa, H. I.; Chang, C. J.; Long, J. R. *Nature* **2010**, *464*, 1329−1333.

(51) Sun, Y.; Bigi, J. P.; Piro, N. A.; Tang, M. L.; Long, J. R.; Chang, C. J. *J. Am. Chem. Soc.* **2011**, *2*, 9212−9215.

(52) Karunadasa, H. I.; Montalvo, E.; Sun, Y.; Majda, M.; Long, J. R.; Chang, C. J. *Science* **2012**, *335*, 698−702.

(53) Korendovych, I. V.; Kryatov, S. V.; Rybak-Akimova, E. V. *Acc. Chem. Res.* **2007**, *40*, 510−521.

(54) Widger, L. R.; Davies, C. G.; Siegler, M. A.; Troeppner, O.; Jameson, G. N. L.; Ivanoić-Burmazović, I.; Goldberg, D. P. *J. Am. Chem. Soc.* **2013**, *136*, 2699−2702.

(55) Prokop, K. A.; de Visser, S. P.; Goldberg, D. P. *Angew. Chem., Int. Ed.* **2010**, *49*, 5091−5095.

(56) Neu, H. M.; Quesne, M. G.; Yang, T.; Prokop-Prigge, K. A.; Lancaster, K. M.; Donohoe, J.; DeBeer, S.; de Visser, S. P.; Goldberg, D. P. *Chem.—Eur. J.* **2014**, *20*, 14584−14588.

(57) Neu, H. M.; Yang, T.; Baglia, R. A.; Yosca, T. H.; Green, M. T.; Quesne, M. G.; de Visser, S. P.; Goldberg, D. P. *J. Am. Chem. Soc.* **2014**, *136*, 13845−13852.

(58) Takahashi, A.; Yamaki, D.; Ikemura, K.; Kurahashi, T.; Ogura, T.; Hada, M.; Fujii, H. *Inorg. Chem.* **2012**, *51*, 7296−7305.

(59) Jeon, I.-R.; Park, J. G.; Haney, C. R.; Harris, T. D. *Chem. Sci.* **2014**, *5*, 2461−2465.

(60) Hansch, C.; Leo, A.; Taft, R. W. *Chem. Rev.* **1991**, *91*, 165−195.

(61) Goldsmith, C. R.; Stack, T. D. P. *Inorg. Chem.* **2006**, *45*, 6048−6055.

(62) Jonas, R. T.; Stack, T. D. P. *J. Am. Chem. Soc.* **1997**, *119*, 8566−8567.

(63) Gütlich, P.; Bill, E.; Trautwein, A. X.; Gütlich, P.; Link, R.; Trautwein, A. *Mössbauer Spectroscopy and Transition Metal Chemistry: Fundamentals and Application*; Springer: Berlin, 2011.

(64) Fillol, J. L.; Codolà, Z.; Garcia-Bosch, I.; Gómez, L.; Pla, J. J.; Costas, M. *Nat. Chem.* **2011**, *3*, 807−813.

(65) Kotani, H.; Suenobu, T.; Lee, Y.-M.; Nam, W.; Fukuzumi, S. *J. Am. Chem. Soc.* **2011**, *133*, 3249−3251.

(66) Hirai, Y.; Kojima, T.; Mizutani, Y.; Shiota, Y.; Yoshizawa, K.; Fukuzumi, S. *Angew. Chem., Int. Ed.* **2008**, *47*, 5772−5776.